



Upper mantle structure beneath the Arabian Peninsula and northern Red Sea from teleseismic body wave tomography: Implications for the origin of Cenozoic uplift and volcanism in the Arabian Shield

Yongcheol Park and Andrew A. Nyblade

Department of Geosciences, Pennsylvania State University, 444 Deike Building, University Park, Pennsylvania 16802, USA (ypark@geosc.psu.edu)

Arthur J. Rodgers

Lawrence Livermore National Laboratory, Geophysics and Global Security Division, P.O. Box 808, Livermore, California 94551-9900, USA

Abdullah Al-Amri

Geology Department and Seismic Studies Center, King Saud University, P.O. Box 2455, 11451 Riyadh, Saudi Arabia

[1] Upper mantle structure between 150 and 400 km depth is imaged beneath the Arabian Shield and northern Red Sea by modeling P and S traveltime residuals from teleseismic events recorded on the Saudi Arabia National Digital Seismic Network, the 1995–1997 Saudi Arabian PASSCAL experiment, and three permanent stations (RAYN, EIL, and MRNI). Relative traveltime residuals were obtained using a multichannel cross-correlation method and inverted for upper mantle structure using VanDecar's inversion method. The resulting images reveal a low-velocity region ($\sim 1.5\%$ for the P model and $\sim 3\%$ for the S model) trending NW–SE along the western side of the Arabian Shield and broadening to the northeast beneath the Makkah-Madinah-Nafud volcanic line. We attribute the low velocities to a mantle thermal anomaly that could be as large as 330 K and that is associated with the Cenozoic uplift of and volcanic centers on the Shield. Our tomographic images are not consistent with models invoking separate mantle upwellings beneath the northern and southern regions of the Shield and instead favor single plume or superplume models. We also find little evidence for low velocities beneath the northern Red Sea, suggesting that there might not be a geodynamic link between rifting in the Red Sea and plateau uplift and volcanism in the Shield.

Components: 6211 words, 10 figures.

Keywords: body wave velocity; tomography; mantle plume; Arabian Shield.

Index Terms: 7270 Seismology: Tomography (6982, 8180); 8121 Tectonophysics: Dynamics: convection currents, and mantle plumes; 7203 Seismology: Body waves.

Received 22 December 2006; **Revised** 19 April 2007; **Accepted** 4 May 2007; **Published** 30 June 2007.

Park, Y., A. A. Nyblade, A. J. Rodgers, and A. Al-Amri (2007), Upper mantle structure beneath the Arabian Peninsula and northern Red Sea from teleseismic body wave tomography: Implications for the origin of Cenozoic uplift and volcanism in the Arabian Shield, *Geochem. Geophys. Geosyst.*, 8, Q06021, doi:10.1029/2006GC001566.

1. Introduction

[2] In this paper, we report results from a study of upper mantle structure beneath the Arabian Shield, and parts of the Arabian Platform and Red Sea using body wave traveltimes tomography (Figure 1). Data used for this study come primarily from the Saudi Arabia National Digital Seismic Network (SANDSN), which has been operated since 1998 by the King Abdulaziz City for Science and Technology (KACST) [Al-Amri and Al-Amri, 1999]. The network consists of 32 stations mostly distributed across the Arabian Shield (Figure 1), twenty-two of which are equipped with broadband (Streckeisen STS-2) seismometers. Five years of data (1999–2003) from the network were provided for this study.

[3] The basement of the study region consists of an amalgamation of Neoproterozoic terrains, and throughout the Arabian Shield these terrains have been subjected to Cenozoic uplift and volcanism. The locations of Tertiary and Quaternary volcanic regions are shown in Figure 1. The oldest volcanic rocks on the Shield (circa 20–30 Ma [Camp et al., 1991; Coleman and McGuire, 1988; Mohr et al., 1988]) are contemporaneous with flood basalt volcanism in Yemen, Afar, and the Ethiopian Plateau, as well as the initiation of rifting in the Red Sea. Younger volcanic rocks (circa 12 Ma to present [Camp and Roobol, 1992; McGuire and Bohannon, 1989]), including a chain of eruptive centers called the Makkah-Madinah-Nafud (MMN) volcanic line, are found in the central and northern parts of the Shield (Figure 1). The average elevation of the Shield is 1 km, but in some areas near the Red Sea, such as the Asir Province in southwestern Saudi Arabia, elevations are as high as 3 km (Figure 1). The uplift of the Arabian Shield probably occurred between 20 and 13 Ma, post-dating the onset of rifting in the Red Sea by at least 10 Ma [Almond, 1986; Bohannon et al., 1989; Dixon et al., 1989; McGuire and Bohannon, 1989].

[4] Although a great deal of work has been done to investigate the origin of Cenozoic uplift and volcanism in the Arabian Shield, the development of these features in relation to rifting in the Red Sea remains poorly understood. The uplift of the Shield and the volcanism on it are generally assumed to be the result of hot, buoyant material in the upper mantle that may have eroded the base of the lithosphere [e.g., Camp and Roobol, 1992; McGuire and Bohannon, 1989]. However, the lateral and vertical extent of the thermal anomaly

in the upper mantle under the Shield is uncertain, as well as its relationship to mantle structure under the Red Sea.

[5] Previous seismic work in the region has revealed low seismic velocities in the upper mantle beneath the Shield, consistent with the presence of a broad thermal anomaly [e.g., Al-Damegh et al., 2005; Al-Lazki et al., 2004; Benoit et al., 2003; Debayle et al., 2001; Julia et al., 2003; Kumar et al., 2002; Mellors et al., 1999; Rodgers et al., 1999; Sandvol et al., 1998, 2001; Tkalčić et al., 2006; Villaseñor et al., 2001]. Some global and regional tomographic studies suggest that the low velocities could extend from shallow upper mantle depths downward across the transition zone and into the lower mantle [e.g., Debayle et al., 2001; Ritsema et al., 1999; Zhao, 2001], which led Daradich et al. [2003] to propose that the uplift of the Shield could be caused by thermally buoyant mantle rock extending from the Moho all the way down into the lower mantle. Other studies, however, have found little evidence for thinning of the transition zone under the Shield [e.g., Benoit et al., 2003; Kumar et al., 2002], suggesting that a thermal anomaly does not extend as deep as the mantle transition zone.

[6] Further evidence for thermally perturbed upper mantle beneath the Shield comes from a recently published study of shear wave splitting using data from the SANDSN [Hansen et al., 2006]. The results of this study show a N–S fast polarization direction for SKS waves across the Shield, as did Wolfe et al. [1999] for the Saudi Arabian PASS-CAL experiment [Vernon et al., 1996]. The generally N–S pattern of fast polarization directions is not easy to explain by flow in the mantle in the direction of plate motion or to fossil anisotropy in the Precambrian lithosphere, and consequently Hansen et al. [2006] attributed the pattern to a combination of plate and density driven flow in the asthenosphere. The density driven flow is believed to be caused by warm material from the Afar hot spot flowing to the northwest channeled by the thinner lithosphere under the Red Sea and the western edge of the Shield. Estimates of plate motion show that the Arabian plate is moving in a northeasterly direction (N40°E) [McClusky et al., 2003; Reilinger et al., 1997].

[7] Given the uncertainty in the nature of the thermal anomaly beneath the Arabian Shield, in this study we investigate it further by tomographically imaging the P and S wave velocity structure of upper mantle. In the next two sections of the

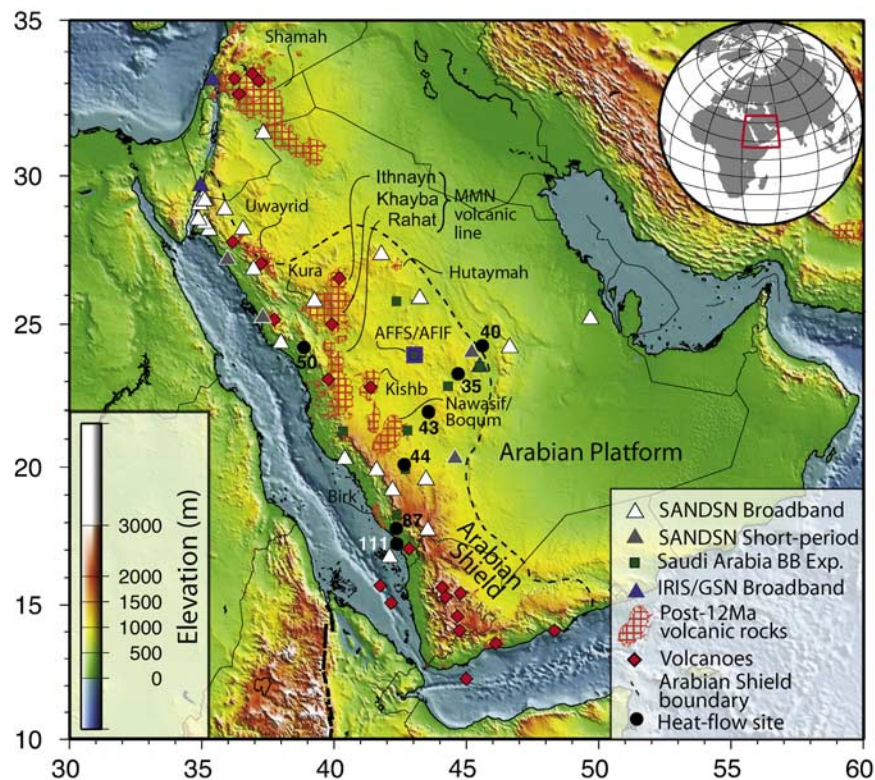


Figure 1. Map of the study area showing topography, seismic station locations, and major tectonic features. Broadband and short period seismic stations of the SANDSN are denoted by white and grey triangles, respectively. The 1995–1997 PASSCAL Broadband Seismic Experiment stations are represented by green squares, and the IRIS/GSN broadband station locations are shown as blue triangles. Co-located stations (AFFS and AFIF) are highlighted with a thick blue line. Black circles indicate heat flow measurements with values in mWm^{-2} [Gettings, 1982]. Red diamonds and red crossing-line pattern represent volcanoes and post-12 Ma volcanic fields, respectively. The outline of the Arabian Shield is shown with the black dashed line.

paper, we describe the data and tomographic modeling procedure used, and also the resolution of the tomographic models. Following that is a discussion of what new insights the models provide about the thermal anomaly, in particular with regard to the Cenozoic uplift and volcanism in the Shield and structure beneath the Red Sea.

2. Data and Traveltime Residuals

[8] As mentioned briefly in the introduction, the data used in this study were obtained mostly from the SANDSN, consisting of twenty-two broadband and eleven short-period seismographs (Figure 1). In addition to the SANDSN data, we have used data from permanent stations in the region (RAYN, EIL and MRNI) and from the Saudi Arabian PASSCAL experiment, which consisted of nine broadband seismic stations deployed for 18 months

between late 1995 and early 1997 (Figure 1) [Vernon *et al.*, 1996].

[9] To check for biases in traveltime residuals between the data sets, we computed traveltime residuals with respect to theoretical traveltimes predicted by the iasp91 model [Kennett and Engdahl, 1991] for many events recorded on a pair of common stations to all three data sets (AFFS and AFIF, Figure 1). Traveltime residuals for events from similar back azimuths and great circle distances do not reveal any systematic bias between the data sets, and we therefore simply combined all of the traveltime observations for the inversion (Figure 2).

[10] The combined data set provides 3889 raypaths with P and PKP wave arrivals from 462 events, and 1777 raypaths with S and SKS wave arrivals from 265 events. The majority of the events are located between back azimuths of 15 and 130 degrees, but

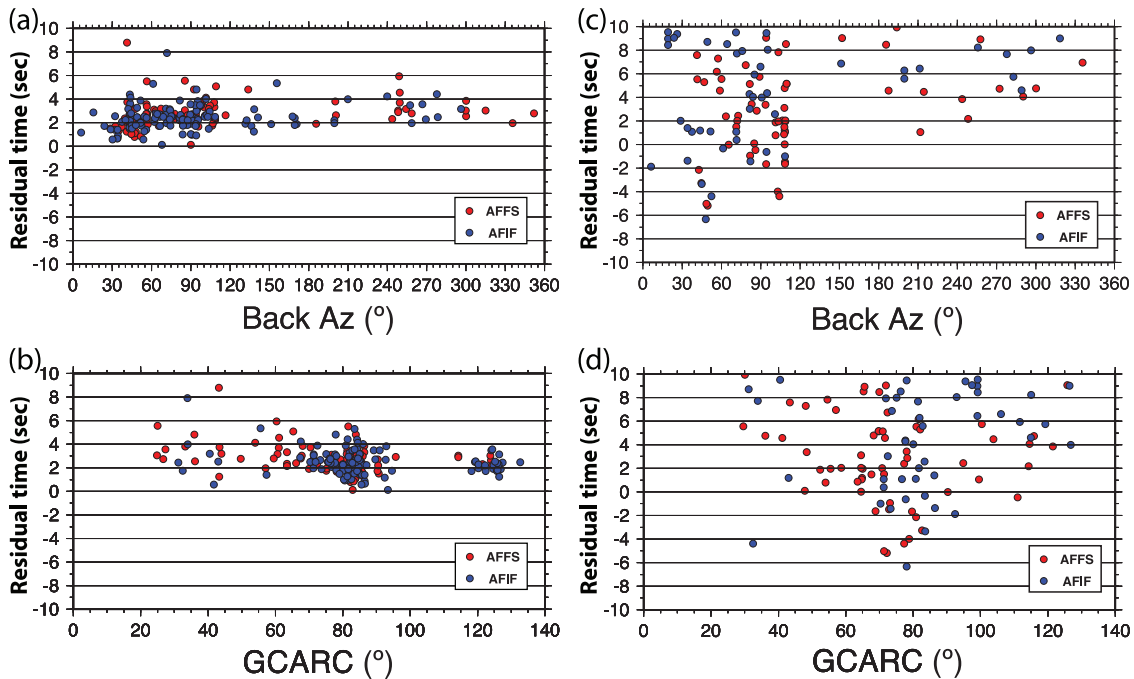


Figure 2. P and S wave traveltime residuals plotted against back azimuths and great circle distances for events recorded on co-located stations AFFS and AFIF for (a and b) P waves and (c and d) S waves.

the events are distributed over a wide range of back azimuths (Figure 3). The waveforms were filtered with a zero-phase two-pole Butterworth filter between 0.5 to 2 Hz for P waves and between 0.04 to

0.1 Hz for S waves. Relative P and S wave traveltime residuals were then computed using the multichannel cross correlation (MCCC) method of *VanDecar and Crosson [1990]*. Figure 4 shows

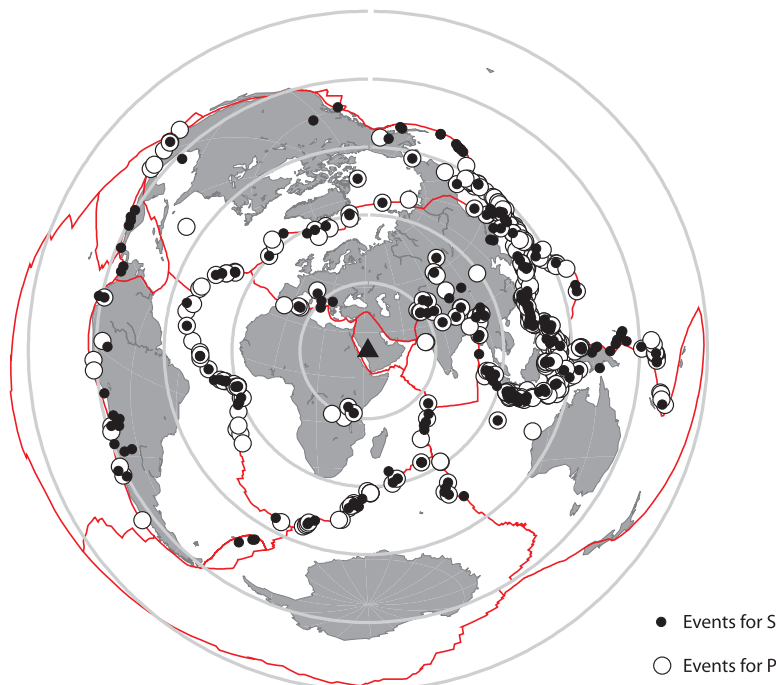


Figure 3. The distribution of earthquakes for P and S wave tomography plotted using an equal distance projection. The red solid lines show major plate boundaries, and the grey circles are at 30-degree distance intervals from the center of the seismic array.

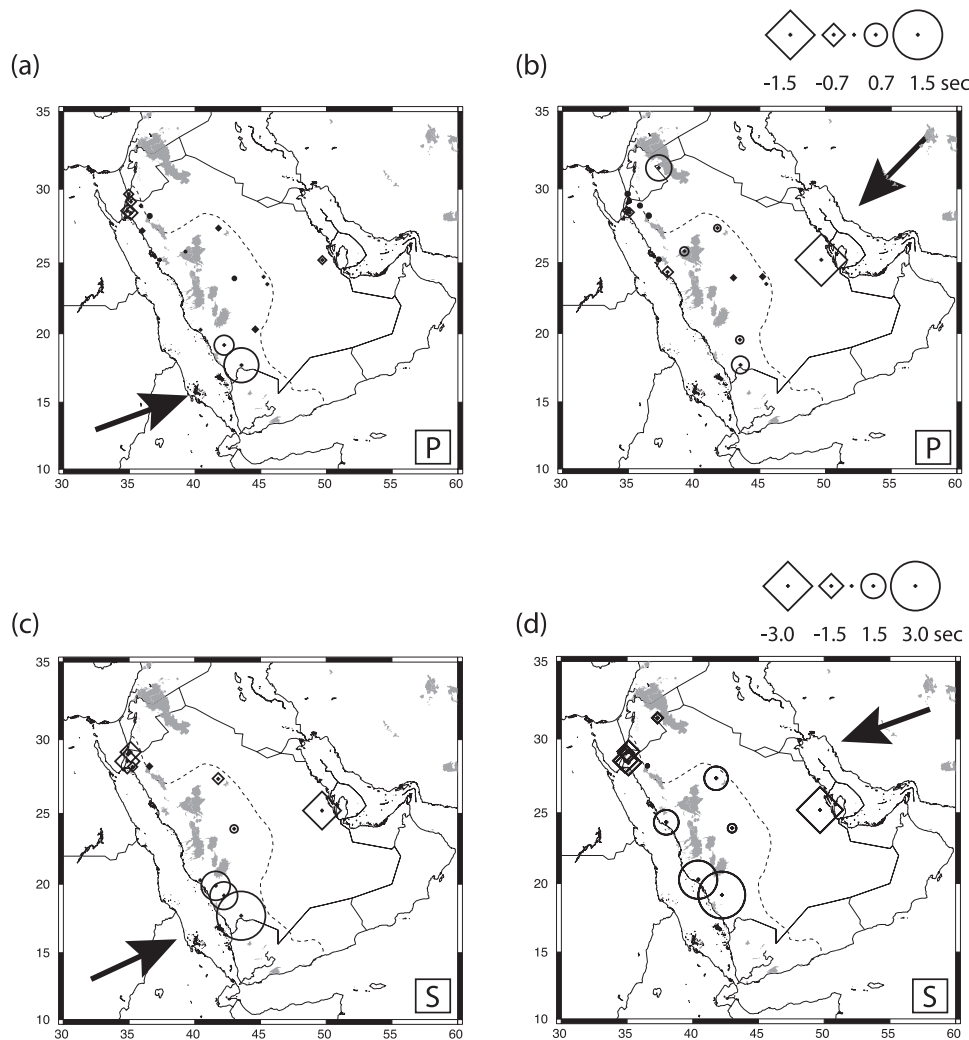


Figure 4. Maps of (a and b) P wave and (c and d) S wave relative arrival-time residuals with different back azimuth. Circles and diamonds represent the stations where observed arrival time is relatively late (positive) and early (negative), respectively. Shaded areas show post-12 Ma volcanic areas. Arrows represent azimuthal direction from the event location to the center of the network.

P and S wave relative arrival-time residuals computed with rays coming from eastern and western azimuths. The relative traveltime residuals for the P and S waves show similar distributions of earlier and later arrivals. Later arrivals (~ 1.5 s for P and 3.0 s for S) are observed on stations located on the western side of the Arabian Shield near the Rea Sea, and earlier arrivals (~ -1.5 s for P and -3.0 s for S) are observed on stations in the Platform (Figure 4).

[11] The traveltime residuals were inverted for a 3-D velocity model using *VanDecar's* [1991] method and a grid consisting of 34 knots in depth, 56 knots in latitude between 12.0°N and 37.0°N and 56 knots in longitude between 29.5°E

and 55.0°E . For the inner region of the model domain (17.4°N – 30.7°N , 35.5°E – 48.5°E , and 0–200 km depth) the horizontal knot spacing in the grid is one third of a degree, and the vertical knot spacing is 25 km. For the outer regions of the model, the vertical knot spacing is 50 km between 200 and 800 km depth, and 100 km between 800 and 1000 km depth. The horizontal knot spacing increases from 0.5 to 1.5 degrees from the next-to-inner region to the outermost region. The *iasp91* model [*Kennett and Engdahl*, 1991] was used for the starting model. *VanDecar and Snieder* [1994] show that model results are not affect by the choice of starting model provided

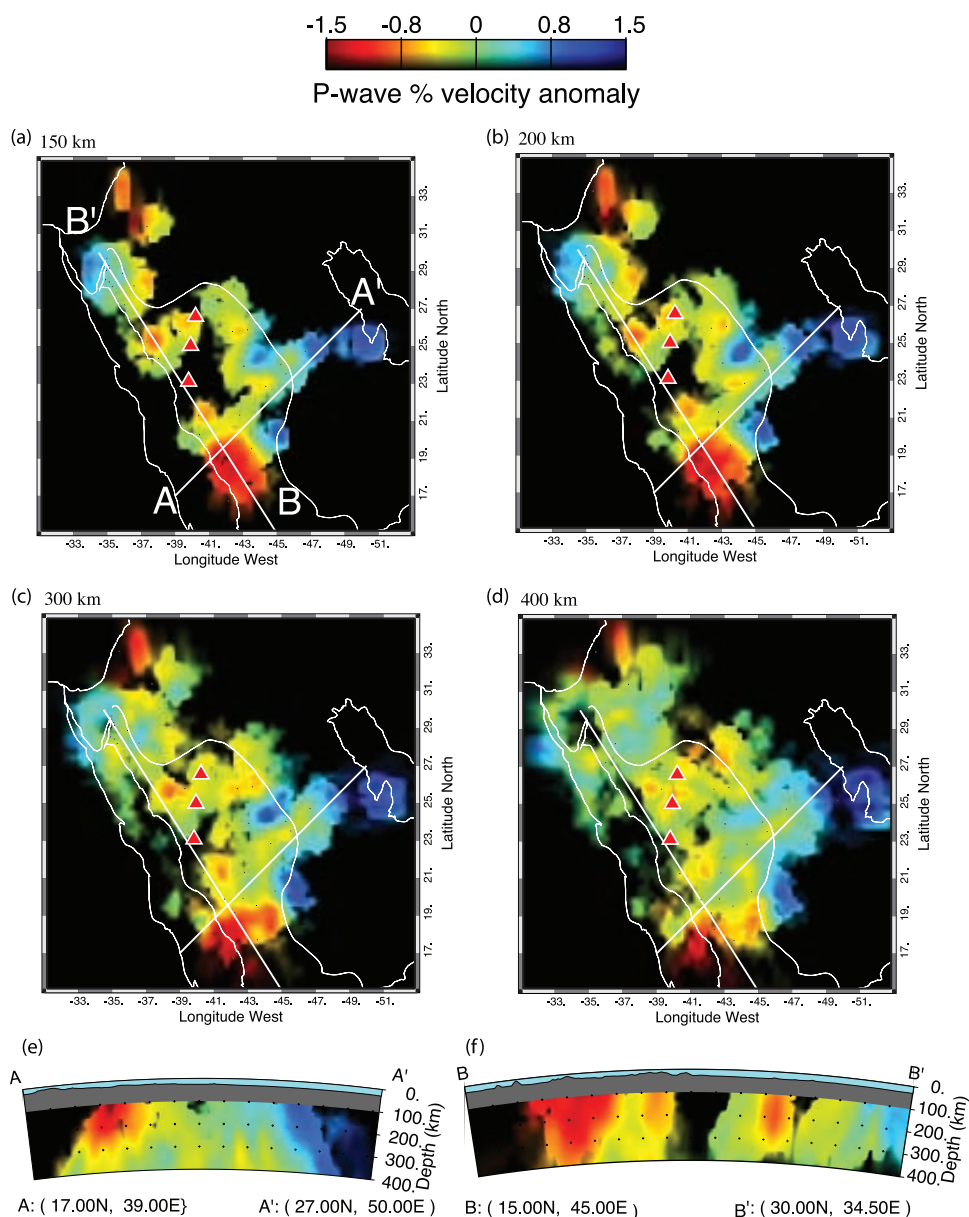


Figure 5. P wave velocity model. (a–d) Horizontal slices through the model are shown for depths of 150, 200, 300, and 400 km, and (e and f) vertical slices are shown for two profiles (A–A' and B–B') whose locations are given in Figure 5a. Areas with a hit count of ≤ 4 are darkened. Red triangles represent the MMN volcanic line. Outlines of the Arabian Shield, the Red Sea, and the Persian Gulf are shown with thin white lines.

that a sufficient number of iterations are used with a regularization of damping.

[12] In the inversion procedure, station static terms can be computed to compensate for traveltime residuals arising from variations in crustal and uppermost mantle structure directly beneath each station, and source terms can be computed to account for structure effects outside the model domain plus event mislocations. To examine the effects of the station and source terms on the model

results, we inverted both P and S wave data sets with and without these terms. The results from the tests are similar for depths between 150 km and 400 km, and we have therefore opted to use the results from the models without station and source terms for our interpretation (see Figures 5 and 6 and auxiliary material Figures S1 and S2 for comparison¹).

¹Auxiliary materials are available in the HTML. doi:10.1029/2006GC001566.

[13] Optimum smoothing and flattening parameters for the inversion were selected through an investigation of trade-off curves of relative traveltimes RMS misfit versus model roughness. The final P wave model results in an RMS traveltimes residual of 0.0213 s, corresponding to a 96% RMS reduction. The final S wave model has a residual reduction of 0.0541 s, accounting for 92% of the RMS residuals. These final residuals for the P and S wave models are on the order of the estimated error from the MCCC of ~ 0.02 s for P waves and ~ 0.05 s for S waves, respectively.

3. Body Wave Tomographic Models

[14] Figure 5 shows depth slices and cross sections through the P wave velocity model obtained from the inversion. Structure below 400 km depth and above 150 km depth is not shown because of the limited number of crossing raypaths below and above the 150–400 km depth interval.

[15] The depth slices (Figures 5a–5d) show low-velocity anomalies of up to $\delta V_p = \sim 1.5\%$ which are confined mainly to the Arabian Shield, with the largest amplitude anomaly located beneath the southwestern part of the Shield. The low-velocity anomaly trends NW–SE beneath the western side of the Shield and broadens to the northeast under MMN volcanic line. A low-velocity zone does not appear at any depths beneath the northern section of the Red Sea (including the Gulfs of Suez and Aqaba). Elsewhere beneath the Red Sea resolution is too poor to interpret upper mantle structure (see section 4).

[16] There is good agreement between the S and P models. The region of low velocities imaged in the P wave model under the western side of the Shield can also be seen in the S wave model with the largest amplitude anomaly ($\sim -3.0\%$) found beneath the southwestern part of the Shield (Figure 6). Also similar to the P wave model, a low-velocity region is not observed beneath the northern part of the Red Sea.

[17] Profile A–A' (Figures 5e and 6e) shows the velocity contrast between the lower-than-average velocities under the western side of the Arabian Shield and higher-than-average velocities under the eastern side of the Shield, as well as under the Arabian platform. Across this profile there is a $\sim 3\%$ and $\sim 6\%$ lateral variation in the P wave and S wave velocities, respectively, between depths of 200–400 km. The vertical slices B–B' in Figures 5f and 6f show strong low-velocity anomalies beneath

the southern and middle parts of the Shield along the Red Sea coast, but not extending north of $\sim 27^\circ\text{N}$ latitude.

4. Resolution Tests

[18] To examine model resolution, we performed a number of tests. The results for checkerboard tests consisting of 100 km diameter spheres with a $\pm 5\%$ slowness anomaly placed at 200, 300, and 400 km depths are shown in Figures 7 and 8. For these tests, noise was added to synthetic traveltimes, obtained by ray tracing through the models, as a Gaussian residual time error with a standard deviation of 0.02 s for synthetic P waves and 0.05 s for S waves.

[19] The recovered models illustrate the horizontal resolution (Figures 7b–7d for P wave model and Figures 8b–8d for S wave model). In the P wave model, the checkerboard anomaly between depths of 200 and 400 km is recovered beneath most parts of the Shield, indicating lateral resolution of ~ 100 km beneath much of the Shield. For the Red Sea, only structure under the northern part can be resolved. Horizontal resolution for the S model is similar to or perhaps slightly better at some depths than for the P model. For example, structure over a wider part of the northern Red Sea (the Sinai Peninsula and the Gulf of Aqaba) can be resolved in the 200–400 km depth interval in the S model compared to the P model.

[20] We also performed a resolution test with low-velocity slabs to investigate the vertical resolution of the models. The input models used for this test consisted of a 100 km-wide slab extending 200 km in depth along the western side of the Shield, with a second shorter slab extending to the northeast beneath the MMN volcanic line (Figures 9a–9c and 10a–10c). The recovered models are shown in Figures 9d–9g and 10d–10g. The amplitudes of the recovered slowness anomalies are only $\sim 36\%$ of the input anomaly, but this is similar to results from other studies using VanDecar's inversion method [e.g., *Bastow et al.*, 2005; *Benoit et al.*, 2006b]. Both the P and S wave models can resolve the horizontal dimensions of the input slab-like low-velocity anomalies clearly. However, the test indicates that the depth resolution of the models is very limited, with the low-velocity anomalies smearing downward by hundreds of kilometers (Figures 9f–9g and 10f–10g). The test also indicates that it is possible to infer from our models (Figures 5 and 6) that a continuous low-velocity

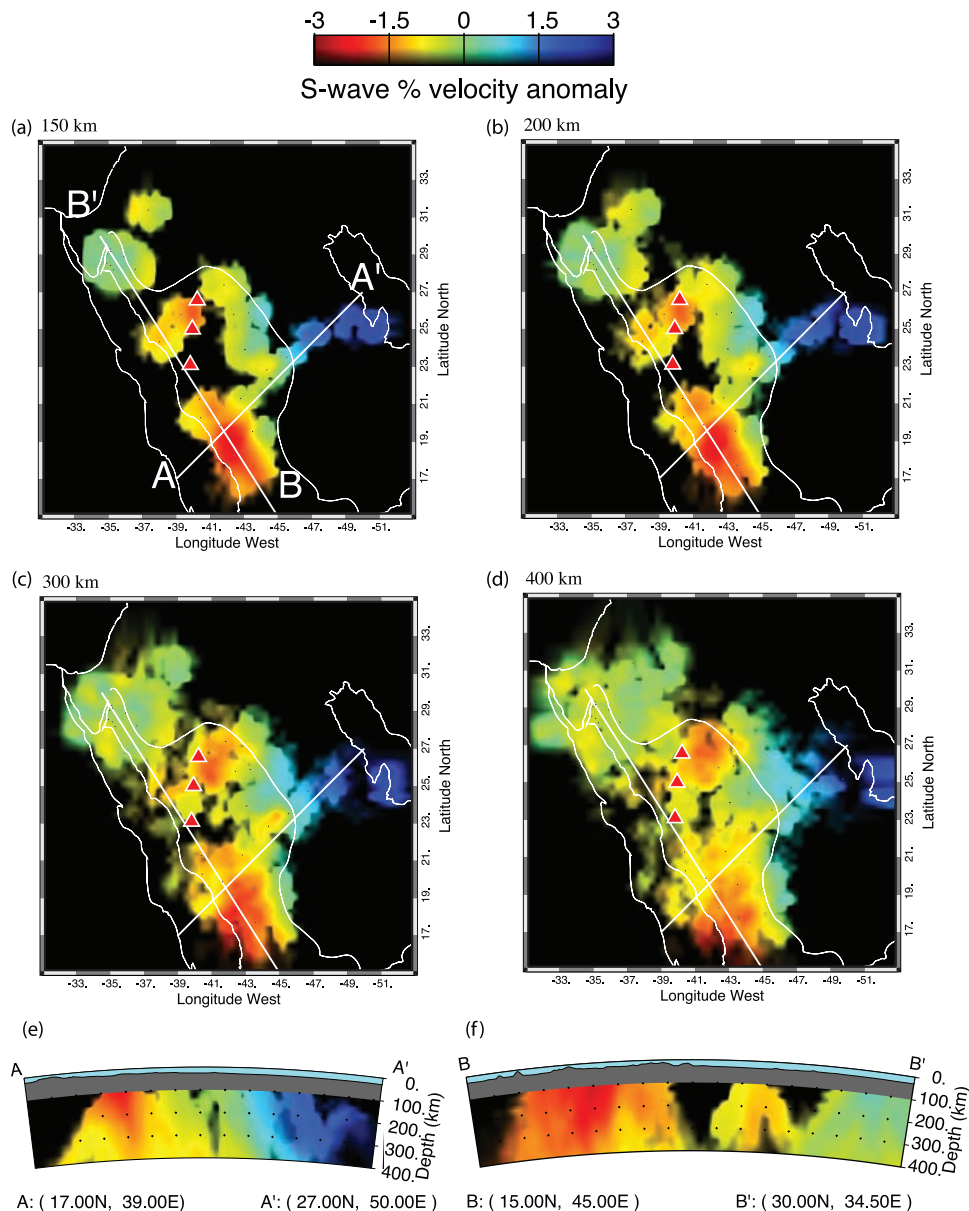


Figure 6. S wave velocity model. (a–d) Horizontal slices through the model are shown for depths of 150, 200, 300, and 400 km, and (e and f) vertical cross sections are shown for two profiles (A–A' and B–B') whose locations are given in Figure 6a. Areas with a hit count of ≤ 4 are darkened. Red triangles represent the MMN volcanic line. Outlines of the Arabian Shield, the Red Sea, and the Persian Gulf are shown with thin white lines.

anomaly exists under the western side of the Shield, and broadens to the northeast under the MMN volcanic line.

5. Discussion

[21] In this section, we discuss how our models compare to previous studies of the region and what new insights can be obtained from them regarding the origin of the Cenozoic uplift and volcanism in

the Shield and the development of the Red Sea. As noted previously, the main feature in our model is a low-velocity anomaly that is most pronounced beneath the southwestern part of the Arabian Shield and that trends NW–SE along the western side of the Shield, broadening to the northeast beneath the MMN volcanic line. The higher amplitude anomaly in the southwestern corner of the Shield is coincident with the high topography of the Asir Province (~ 3000 m).

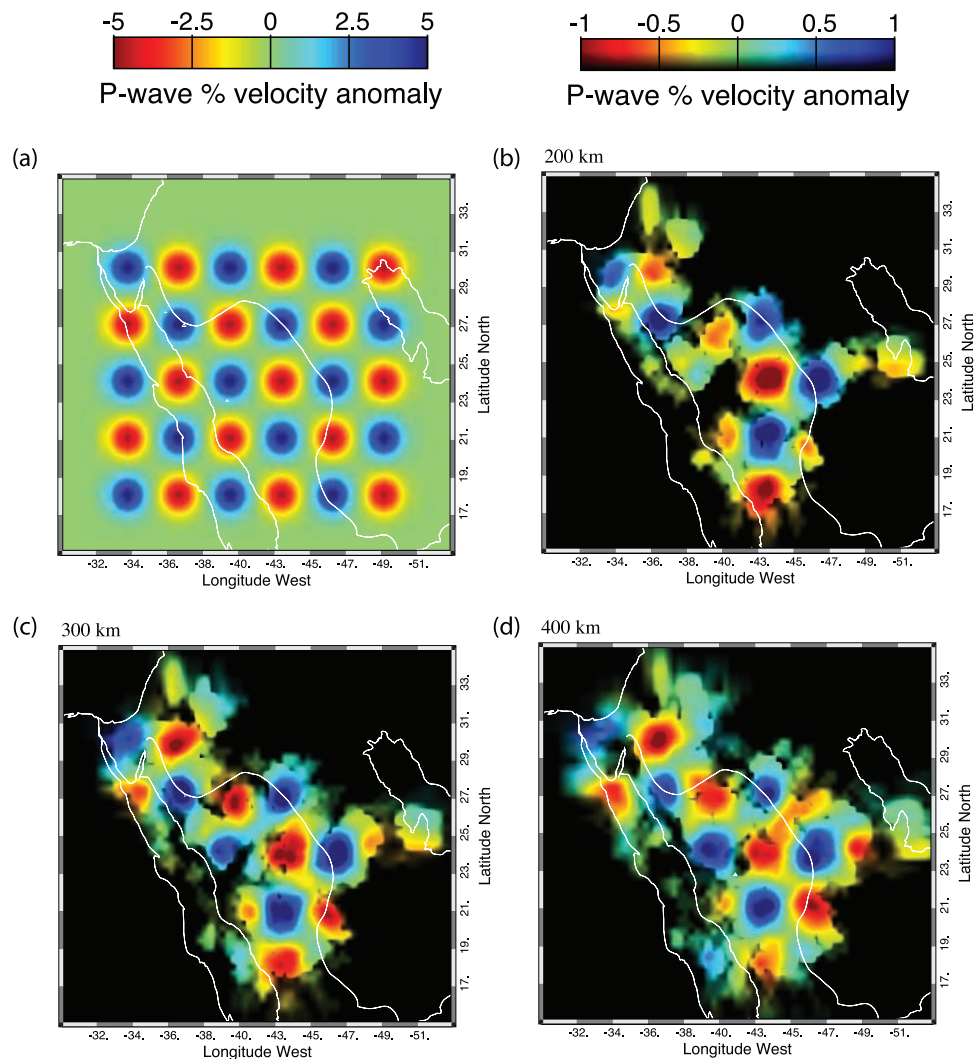


Figure 7. Synthetic checkerboard resolution test for the P wave model. One hundred kilometer diameter Gaussian spheres with $\pm 5\%$ peak velocity anomaly are distributed in a layer at depths of 200, 300, and 400 km. (a) Input checkerboard model for each depth. (b–d) Recovered models.

[22] The low-velocity anomaly imaged is broadly consistent with models of upper mantle structure for depths $> \sim 150$ km reported in other global and continental-scale tomographic studies [e.g., *Benoit et al.*, 2003; *Debayle et al.*, 2001; *Maggi and Priestley*, 2005; *Ritsema and van Heijst*, 2000; *Ritsema et al.*, 1999]. However, our model varies in some important ways, in that not all of the previously published models show (1) a low-velocity anomaly under the northern part of the Shield coincident with the MMN volcanic line or (2) an absence of a low-velocity anomaly beneath the northern part of the Red Sea.

[23] As for shallower ($\leq \sim 150$ km depth) structure, there is generally good correlation between the low-velocity regions in our model with regions of

inefficient Pn [*Al-Lazki et al.*, 2004; *Mellors et al.*, 1999] and Sn propagation [*Al-Damegh et al.*, 2005; *Mellors et al.*, 1999; *Sandvol et al.*, 2001]. From regional waveform modeling, *Rodgers et al.* [1999] found that P and S wave velocities below the Moho are slower in the Shield than in the Platform and that Poisson's ratio is higher (0.29 in the Shield and 0.27 in the Platform). Receiver function studies [*Kumar et al.*, 2002] and joint inversions between receiver functions and surface wave group velocities [*Julia et al.*, 2003; *Tkalčić et al.*, 2006] show thermally perturbed Shield lithosphere underlain by a low-velocity zone. These comparisons indicate that the anomalous upper mantle structure seen in Figures 5 and 6 beneath the Shield in the 200–400 km depth interval is present at uppermost mantle depths as well.

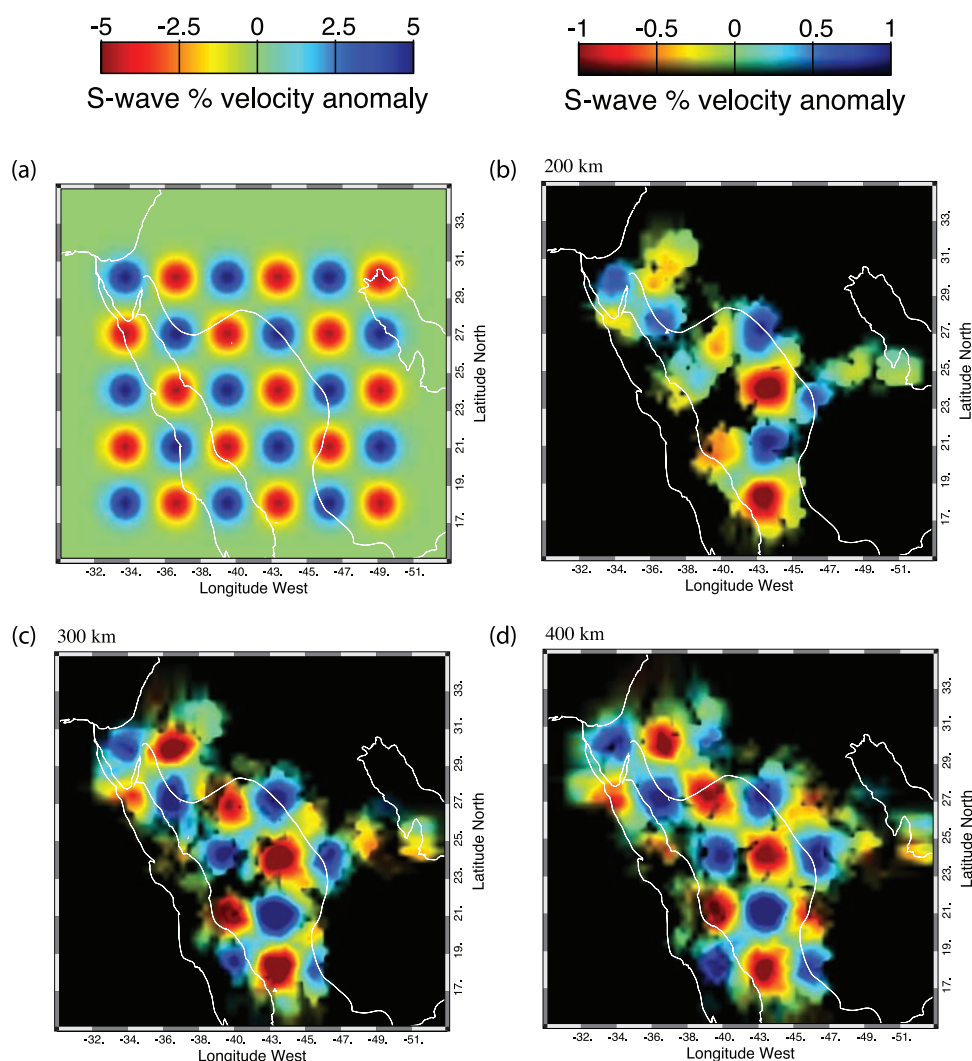


Figure 8. Synthetic checkerboard resolution test for the S wave model. One hundred kilometer diameter Gaussian spheres with $\pm 5\%$ peak velocity anomaly are distributed in a layer at depths of 200, 300, and 400 km. (a) Input checkerboard model for each depth. (b–d) Recovered models.

[24] The temperature perturbation needed to explain the low-velocity anomaly in our S wave model can be estimated using the method of *Faul and Jackson* [2005], which yields a temperature derivative of ~ 1.2 m/s/K at an average temperature of 1300°C for a 10 mm upper mantle grain size. The resolution tests suggest that the magnitude of the low-velocity anomaly in our S wave model could be underestimated by a factor of three, and thus the observed low-velocity anomaly of $\sim -3\%$ beneath the Shield area could be as large as 9% . Using a temperature derivative of 1.2 m/s/K and the relative velocity perturbation in our models, a relative temperature variation can be computed. A 9% reduction in S wave velocity can be achieved by a 330 K increase in temperature, whereas a 3% reduction can be achieved by a 115 K temperature

increase. The maximum temperature estimate of 330 K suggests that partial melts could be present in the upper mantle beneath the Arabian Shield [*Sato et al.*, 1988], consistent with the presence of Holocene volcanic activity. Heat flow measurements from the Shield (Figure 1) [*Gettings*, 1982], on the other hand, are similar to the global average for Precambrian terrains [*Artemieva and Mooney*, 2001; *Nyblade and Pollack*, 1993], indicating that the thermal anomaly in the upper mantle has not yet propagated to the surface away from the volcanic centers.

[25] Do our models support previous studies suggesting a geodynamic link between the anomalous upper mantle structure under the Shield and the Rea Sea? *Coleman and McGuire* [1988] and

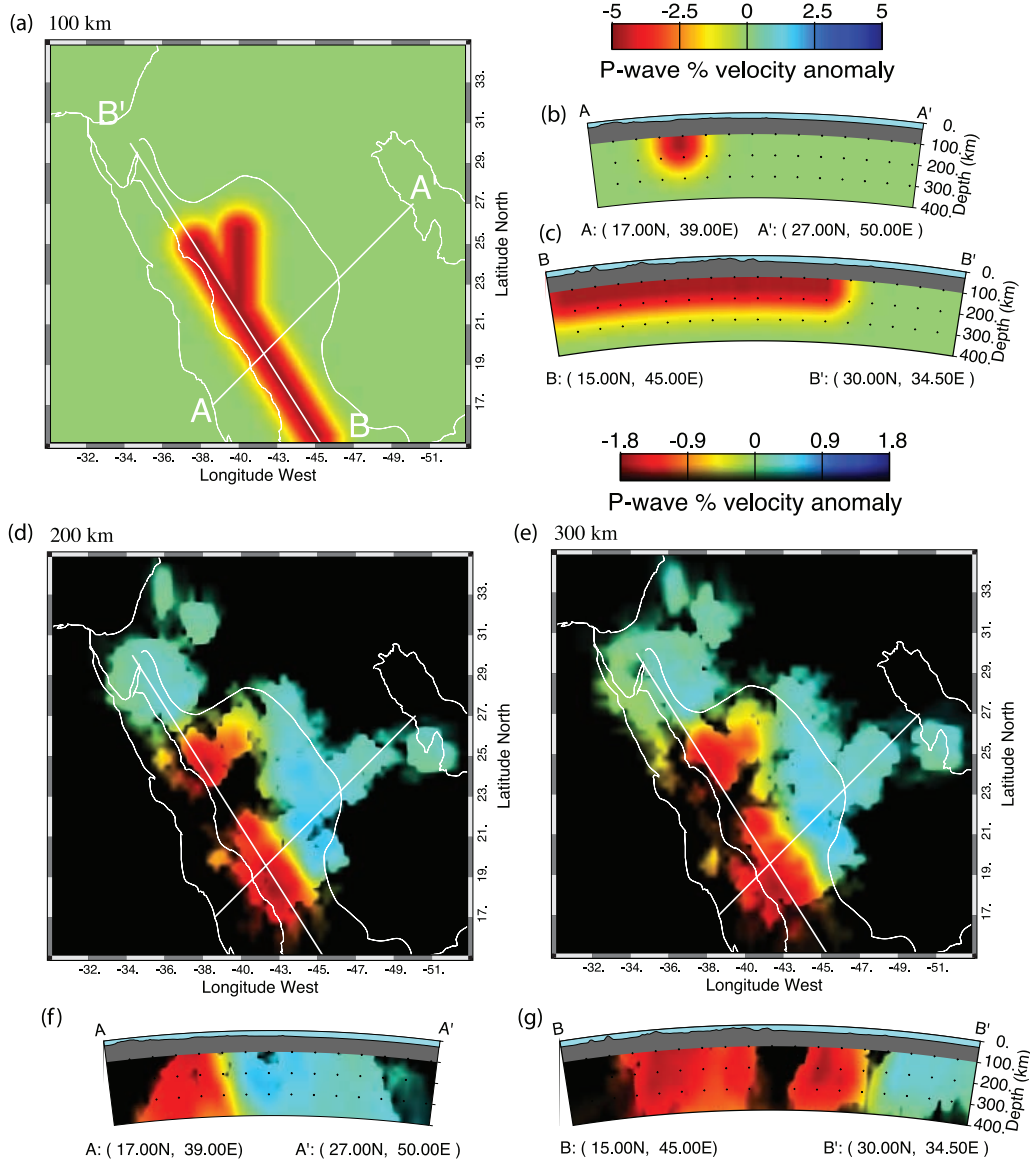


Figure 9. Synthetic slab resolution test for the P wave model. (a–c) Input model showing 100-km wide, 250-km deep low-velocity slabs. (d–g) Recovered model from the inversion: horizontal cross sections at depths of (d) 200 km and (e) 300 km and vertical cross sections along (f) A–A' and (g) B–B'.

McGuire and Bohannon [1989], for example, proposed the existence of partial melting in the upper mantle caused by the advective rise of magma from deep beneath the Shield coupled with flow laterally toward the axis of rifting in the Red Sea. We are unable to image upper mantle structure beneath much of the Red Sea; however, the resolution of our models for the northern section of the Red Sea is reasonably good. Our models show a low-velocity anomaly in the upper mantle extending along the western side of the Shield, but the

anomaly does not extend to the north of $\sim 27^\circ\text{N}$ latitude in the vicinity of the northern Red Sea or Gulf of Aqaba (Figures 5f and 6f). Thus our models do not support a geodynamic connection between upper mantle processes under the Shield and the Red Sea, at least not locally north of $\sim 27^\circ\text{N}$ latitude.

[26] A number of authors have invoked plumes to explain the Cenozoic uplift of the Shield and the volcanism. Camp and Roobol [1992] suggested the

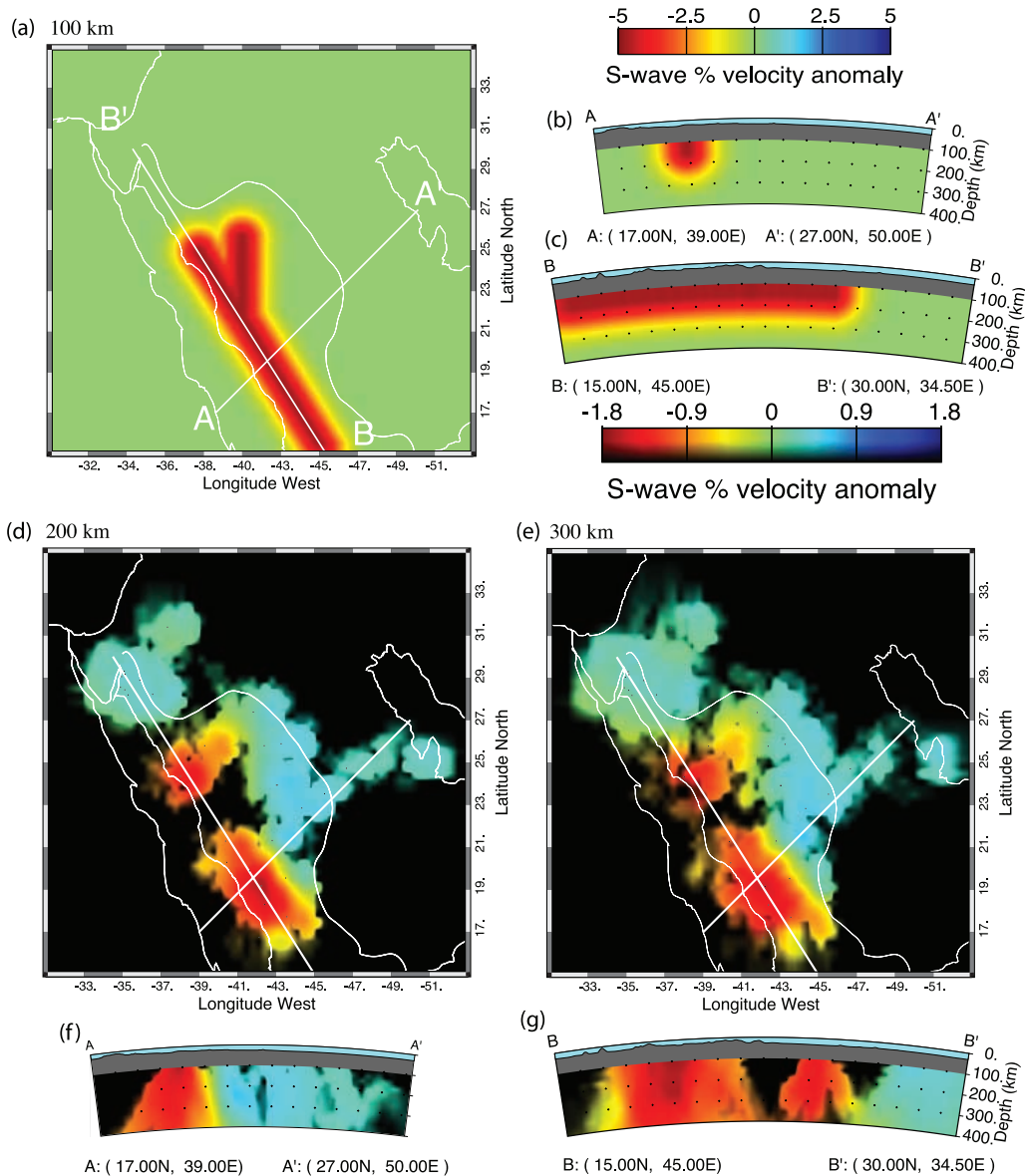


Figure 10. Synthetic slab resolution test for the S wave model. (a–c) Input model showing 100-km wide, 250-km deep low-velocity slabs. (d–g) Recovered model from the inversion: horizontal cross sections at depths of (d) 200 km and (e) 300 km and vertical cross sections along (f) A–A' and (g) B–B'.

existence of a narrow, deep rooted mantle upwelling located beneath the northern part of the Arabian Shield in proximity of the MMN volcanic line and a second one to the south beneath Afar. *Montelli et al.* [2004] imaged a low-velocity structure extending deeper than ~670 km depth beneath the Afar, but their model does not show a thermal anomaly beneath the northern part of the Shield. *Burke* [1996] suggested a multiplume model, in which plumes exist in many places beneath the African and Arabian plates related with topographic swells and volcanic activity. *Ebinger and Sleep*

[1998] proposed a model with a large plume located beneath Ethiopia and flow of warm plume material along the Red Sea coast channeled by topography on the lithosphere-asthenosphere boundary. And from a regional tomographic study, *Debayle et al.* [2001] developed a shear wave velocity model showing a broad low-velocity zone beneath Ethiopia and the southern part of the Red Sea. The low-velocity anomaly in their model is elongated in an E–W direction at deeper depths (>500 km), suggesting the presence of a plume conduit located

beneath the southern part of the Arabian Plate and the Red Sea.

[27] The main feature in our model, a NW–SE trending low-velocity anomaly beneath the western side of the Shield that broadens to the NE under the MMN volcanic line, is not consistent with models invoking two distinct mantle upwelling beneath the Shield [e.g., *Camp and Roobol*, 1992]. The horizontal resolution of our models is sufficient to distinguish between separate low-velocity regions (one north and one south) under the Shield (Figures 7 and 8). The NW–SE trend of the low-velocity anomaly under the western side of the Shield is also not consistent with the plume confined to the Afar region [e.g., *Montelli et al.*, 2004]. The NW–SE trend in the low-velocity anomaly under the western side of the Shield is, however, consistent with the Ebinger and Sleep model proposing plume flow channeled by thinner lithosphere along the Red Sea coast [*Ebinger and Sleep*, 1998].

[28] Another plume-like model for the Shield has been proposed by *Daradich et al.* [2003], who invoked a mantle upwelling originating in the lower mantle beneath southern Africa (the so-called African Superplume) extending to the surface beneath the Arabian Shield. Support for this interpretation comes from some global tomographic images showing the Superplume anomaly rising from mid mantle depths beneath southern and central Africa to the east, connecting with a low-velocity region in the upper mantle beneath eastern Africa and the Arabian Shield [e.g., *Grand*, 2002; *Ritsema et al.*, 1999]. Higher resolution regional tomographic images of upper mantle structure under eastern Africa also show a low-velocity region that extends from shallow upper mantle depths downward into the transition zone and that dips to the west with depth toward central Africa, similar to the global images [*Benoit et al.*, 2006a, 2006b; *Park and Nyblade*, 2006; *Ritsema et al.*, 1998].

[29] The interpretation of *Daradich et al.* [2003] is consistent with our models. The NW–SE low-velocity anomaly beneath the western side of the Shield could be the northern-most extent of the African Superplume structure. *Benoit et al.* [2003] and *Kumar et al.* [2002] found little evidence for thermally perturbed mantle transition zone structure beneath the southern Shield region from stacking receiver functions to image topography on the 410 and 660 km discontinuities. Thus mantle flow associated with the Superplume could be crossing the transition zone beneath Ethiopia, where the 660 km discontinuity is elevated [*Benoit et al.*,

2006a], and flowing to the north in the upper mantle beneath the thinned Shield lithosphere along the Red Sea, not unlike the channeled plume flow in the model of *Ebinger and Sleep* [1998].

6. Summary

[30] Our P and S wave tomographic images reveal a low-velocity region trending NW–SE along the western side of the Arabian Shield but not extending north of $\sim 27^\circ\text{N}$ latitude. The low-velocity region instead broadens to the northeast beneath the MMN volcanic line. The low-velocity region under the Shield can be attributed to a 115–330 K thermal anomaly in the upper mantle, and this anomaly can be associated with the Cenozoic uplift of and volcanic centers on the Shield. Our results do not support the existence of a geodynamic link between upper mantle processes under the Shield and the northern Red Sea. A number of plume models have been proposed to explain the Cenozoic uplift and volcanism on the Shield, including multiple plume heads, a single plume head, and a superplume. Our tomographic images are not consistent with models invoking separate mantle upwellings beneath the northern and southern regions of the Shield and instead favor single plume or superplume models.

Acknowledgments

[31] We thank John VanDecar for use of his MCCC and inversion code and Steve Gao and Susan van der Lee for helpful reviews. This work has been supported by the National Science Foundation (grants EAR 993093, 0003424, and 0505812) and the Department of Energy (contract DE-FC52-05NA26602).

References

- Al-Amri, M., and A. Al-Amri (1999), Configuration of the seismolographic networks in Saudi Arabia, *Seismol. Res. Lett.*, *70*, 322–331.
- Al-Damegh, K., et al. (2005), Crustal structure of the Arabian Plate: New constraints from the analysis of teleseismic receiver functions, *Earth Planet. Sci. Lett.*, *231*, 177–196.
- Al-Lazki, A. I., et al. (2004), Pn tomographic imaging of mantle lid velocity and anisotropy at the junction of the Arabian, Eurasian and African plates, *Geophys. J. Int.*, *158*, 1024–1040.
- Almond, D. C. (1986), The relation of Mesozoic-Cainozoic volcanism to tectonics in the Afro-Arabian Dome, *J. Volcanol. Geotherm. Res.*, *28*, 225–246.
- Artemieva, I. M., and W. D. Mooney (2001), Thermal thickness and evolution of Precambrian lithosphere: A global study, *J. Geophys. Res.*, *106*, 16,387–16,414.
- Bastow, I. D., et al. (2005), Upper-mantle seismic structure in a region of incipient continental breakup: Northern Ethiopian rift, *Geophys. J. Int.*, *162*, 479–493.

- Benoit, M. H., A. A. Nyblade, J. C. VanDecar, and H. Gurrrola (2003), Upper mantle P wave velocity structure and transition zone thickness beneath the Arabian Shield, *Geophys. Res. Lett.*, *30*(10), 1531, doi:10.1029/2002GL016436.
- Benoit, M. H., A. A. Nyblade, T. J. Owens, and G. Stuart (2006a), Mantle transition zone structure and upper mantle S velocity variations beneath Ethiopia: Evidence for a broad, deep-seated thermal anomaly, *Geochem. Geophys. Geosyst.*, *7*, Q11013, doi:10.1029/2006GC001398.
- Benoit, M. H., et al. (2006b), Upper mantle P wave speed variations beneath Ethiopia and the origin of the Afar Hot-spot, *Geology*, *34*, 239–332.
- Bohannon, R. G., et al. (1989), The timing of uplift, volcanism, and rifting peripheral to the Red Sea: A case for passive rifting?, *J. Geophys. Res.*, *94*, 1683–1701.
- Burke, K. (1996), The African Plate, *S. Afr. J. Geol.*, *99*, 341–409.
- Camp, V. E., and M. J. Roobol (1992), Upwelling asthenosphere beneath western Arabia and its regional implications, *J. Geophys. Res.*, *97*, 15,255–15,271.
- Camp, V. E., et al. (1991), Tomographic and volcanic asymmetry around the Red Sea: Constraints on rift models; discussion and reply [modified], *Tectonics*, *10*, 649–656.
- Coleman, R. G., and A. V. McGuire (1988), Magma systems related to the Red Sea opening, *Tectonophysics*, *150*, 77–100.
- Daradich, A., et al. (2003), Mantle flow, dynamic topography, and rift-flank uplift of Arabia, *Geology*, *31*, 901–904.
- Debayle, E., et al. (2001), Seismic evidence for a deeply rooted low-velocity anomaly in the upper mantle beneath the northeastern Afro/Arabian continent, *Earth Planet. Sci. Lett.*, *193*, 423–436.
- Dixon, T., et al. (1989), Topographic and volcanic asymmetry around the Red Sea: Constraints on rift models, *Tectonics*, *8*, 1193–1216.
- Ebinger, C. J., and N. H. Sleep (1998), Cenozoic magmatism throughout east Africa resulting from impact of a single plume, *Nature*, *395*, 788–791.
- Faul, U. H., and I. Jackson (2005), The seismological signature of temperature and grain size variations in the upper mantle, *Earth Planet. Sci. Lett.*, *234*, 119–134.
- Gettings, M. E. (1982), Heat-flow measurements at shot point along the 1978 Saudi Arabian Seismic Deep-Refracton LINE, Part 2: Discussion and interpretation, *U.S. Geol. Surv. Open File Rep.*, 82–794.
- Grand, S. P. (2002), Mantle shear-wave tomography and the fate of subducted slabs, *Philos. Trans. R. Soc. London, Ser. A*, *360*, 2475–2491.
- Hansen, S., et al. (2006), Combined plate motion and density driven flow in the asthenosphere beneath Saudi Arabia: Evidence from shear-wave splitting and seismic anisotropy, *Geology*, *34*, 869–892.
- Julia, J., et al. (2003), Lithospheric structure of the Arabian Shield from the joint inversion of receiver functions and surface-wave group velocities, *Tectonophysics*, *371*, 1–21.
- Kennett, B. N. L., and E. R. Engdahl (1991), Travel times for global earthquake location and phase identification, *Geophys. J. Int.*, *105*, 429–465.
- Kumar, M. R., D. S. Ramesh, J. Saul, D. Sarkar, and R. Kind (2002), Crustal structure and upper mantle stratigraphy of the Arabian shield, *Geophys. Res. Lett.*, *29*(8), 1242, doi:10.1029/2001GL014530.
- Maggi, A., and K. Priestley (2005), Surface waveform tomography of the Turkish-Iranian Plateau, *Geophys. J. Int.*, *160*, 1068–1080.
- McClusky, S., et al. (2003), GPS constraints on Africa (Nubia) and Arabia plate motions, *Geophys. J. Int.*, *155*, 126–138.
- McGuire, A. V., and R. G. Bohannon (1989), Timing of mantle upwelling: Evidence for a passive origin for the Red Sea Rift, *J. Geophys. Res.*, *94*, 1677–1682.
- Mellors, R. J., et al. (1999), Regional waveform propagation in the Arabian Peninsula, *J. Geophys. Res.*, *104*, 20,221–20,235.
- Mohr, P. A., et al. (1988), The Ethiopian flood basalt province, in *Continental Flood Basalts*, edited by J. D. Macdougall, pp. 65–110, Kluwer Acad., Boston, Mass.
- Montelli, R., et al. (2004), Finite-frequency tomography reveals a variety of plumes in the mantle, *Science*, *303*, 338–343.
- Nyblade, A. A., and H. N. Pollack (1993), A global analysis of heat flow from Precambrian terrains: Implications for the thermal structure of Archean and Proterozoic lithosphere, *J. Geophys. Res.*, *98*, 12,207–12,218.
- Park, Y., and A. A. Nyblade (2006), P-wave tomography reveals a westward dipping low velocity zone beneath the Kenya Rift, *Geophys. Res. Lett.*, *33*, L07311, doi:10.1029/2005GL025605.
- Reilinger, R. E., et al. (1997), Global Positioning System measurements of present-day crustal movements in the Arabia-Africa-Eurasia plate collision zone, *J. Geophys. Res.*, *102*, 9983–9999.
- Ritsema, J., and H. van Heijst (2000), New seismic model of the upper mantle beneath Africa, *Geology*, *28*, 63–66.
- Ritsema, J., et al. (1998), Upper mantle seismic velocity structure beneath Tanzania, east Africa: Implications for the stability of cratonic lithosphere, *J. Geophys. Res.*, *103*, 21,201–21,213.
- Ritsema, J., et al. (1999), Complex shear wave velocity structure imaged beneath Africa and Iceland, *Science*, *286*, 1925–1928.
- Rodgers, A. J., et al. (1999), Lithospheric structure of the Arabian Shield and Platform from complete regional waveform modelling and surface wave group velocities, *Geophys. J. Int.*, *138*, 871–878.
- Sandvol, E., et al. (1998), Lithospheric seismic velocity discontinuities beneath the Arabian Shield, *Geophys. Res. Lett.*, *25*, 2873–2876.
- Sandvol, E., et al. (2001), Tomographic imaging of Lg and Sn propagation in the Middle East, *Pure Appl. Geophys.*, *158*, 1121–1163.
- Sato, H., et al. (1988), Thermal structure of the low velocity zone derived from laboratory and seismic investigations, *Geophys. Res. Lett.*, *15*, 1227–1230.
- Tkalčić, H., M. E. Pasyanos, A. J. Rodgers, R. Gök, W. R. Walter, and A. Al-Amri (2006), A multistep approach for joint modeling of surface wave dispersion and teleseismic receiver functions: Implications for lithospheric structure of the Arabian Peninsula, *J. Geophys. Res.*, *111*, B11311, doi:10.1029/2005JB004130.
- VanDecar, J. C. (1991), Upper mantle structure of the Cascadia subduction zone from non-linear teleseismic travel time inversion, Ph.D. thesis, Univ. of Wash., Seattle, Wash.
- VanDecar, J. C., and R. S. Crosson (1990), Determination of teleseismic relative phase arrival times using multi-channel cross-correlation and least-squares, *Bull. Seismol. Soc. Am.*, *80*, 150–169.
- VanDecar, J. C., and R. Snieder (1994), Obtaining smooth solutions to large, linear, inverse problems, *Geophysics*, *59*, 818–829.
- Vernon, F., et al. (1996), Observations from regional and teleseismic earthquakes recorded by a deployment of broadband

- seismometers in the Saudi Arabian Shield, *Eos Trans. AGU*, 77, 478.
- Villaseñor, A., et al. (2001), Shear velocity structure of central Eurasia from inversion of surface wave velocities, *Phys. Earth Planet. Inter.*, 123, 169–184.
- Wolfe, C. J., et al. (1999), Shear-wave splitting across western Saudi Arabia: The pattern of upper mantle anisotropy at a Proterozoic shield, *Geophys. Res. Lett.*, 26, 779–782.
- Zhao, D. (2001), Seismic structure and origin of hotspots and mantle plumes, *Earth Planet. Sci. Lett.*, 192, 251–265.